Structural properties of GeSn thin films grown by molecular beam epitaxy

Z. P. Zhang,[1,2] Y. X. Song,[1,a] Z. Y. S. Zhu,[1,2] Y. Han,[1,3] Q. M. Chen,[1,3]
Y. Y. Li,[1] L. Y. Zhang,[1] and S. M. Wang[1,2,4,a]

[1]*State Key Laboratory of Functional Materials for Informatics, Shanghai Institute of Microsystem and Information Technology, Chinese Academy of Sciences, Shanghai 200050, China*
[2]*School of Physical Science and Technology, ShanghaiTech University, Shanghai 201210, China*
[3]*University of Chinese Academy of Sciences, Beijing 100190, China*
[4]*Department of Microtechnology and Nanoscience, Chalmers University of Technology, Gothenburg 41296, Sweden*

GeSn thin films on Ge (001) with various Sn concentrations from 3.36 to 7.62% were grown by molecular beam epitaxy and characterized. The structural properties were analyzed by reciprocal space mapping in the symmetric (004) and asymmetric (224) planes by high resolution X-ray diffraction (XRD). The lateral correlation length (LCL) and the mosaic spread (MS) were extracted for the epi-layer peaks in the asymmetric (224) diffraction. With the increase of Sn concentration, the LCL reduces while the MS increases, indicating degrading crystalline quality. Dislocations were observed in the sample with 7.62% Sn concentration by transmission electron microscope, consistent with the strain relaxation found in XRD mapping. Besides, the surface morphologies were investigated. © *2017 Author(s). All article content, except where otherwise noted, is licensed under a Creative Commons Attribution (CC BY) license (http://creativecommons.org/licenses/by/4.0/).* [http://dx.doi.org/10.1063/1.4982245]

INTRODUCTION

The silicon (Si) based electronics industry has been developing fast since 1950s.[1] The improved performance of integrated circuits was mostly due to the increasing integration of transistors. To further increase performance, the scaling of microelectronic circuits is driven to be increasingly sophisticated, which in turn leads to a range of challenges, including high costs, high power consumption, quantum limitations, *etc.*[2] Si photonics is one of the most promising solutions to solve these problems, and significant progresses have been demonstrated for many Si-based optical components and integration techniques.[3] The integration of optoelectronics and microelectronics on a single chip can exhibit the advantages of both low power consumption and high speed. Commercial Si photonics products have already been available, for example "a single-mode wavelength-division-multiplexing transceiver" from Kotura.[4]

However, for all the Si photonics circuits available nowadays, the lasers are made of III-V materials and bonded to the Si circuits since Si is an indirect bandgap material, preventing it from emitting light efficiently.[5] The III-V technology is not compatible with the complementary metal-oxide-semiconductor (CMOS) processing platform, and the bonding method hinders the future high density integration. Monolithic light sources on Si compatible with the CMOS technology are highly desired. Ge is also an indirect bandgap semiconductor, but the 136 meV gap between the Γ- and L-valley is much smaller than that of Si.[6] Introducing Sn in Ge forming a GeSn alloy can make transformation of the **L**-valley and **Γ**-valley in the conduction band to convert it into a direct bandgap

---

[a]Corresponding authors: songyuxin@mail.sim.ac.cn, shumin@mail.sim.ac.cn

semiconductor. The bandgap transition occurs when the Sn concentration is above about 7%.[7] GeSn alloy with a high Sn concentration is a promising direct bandgap material for light emission and detection. Besides the tunable bandgap, GeSn alloy is also predicted to hold high electron and hole mobility, which makes it a potential candidate material for both optoelectronic and electronic devices integrated on Si platform,[8] such as high mobility channel MOSFET,[9] infrared (IR) photodetectors,[10] IR light-emitting diodes,[11] IR lasers[12] and so on.

The thermal equilibrium solid solubility of Ge–Sn binary system is as low as 1%.[13] Sn segregation during the growth is the largest challenge for formation of homogeneous GeSn alloys.[14] Molecular beam epitaxy (MBE) and chemical vapor deposition (CVD) are the mostly utilized method for the epitaxy of GeSn alloy. GeSn alloy grown by CVD usually shows better uniformity and crystalline quality than that by MBE.[15] Almost all GeSn samples that are capable of obtaining light emission are grown by CVD, including the first photoluminescence (PL) results,[16] the first GeSn laser,[12] etc. On the other hand, for the GeSn alloys with ultra-high Sn contents are grown by MBE. The non-equilibrium processes during MBE are effective to avoid Sn segregation, achieved by low temperature growth, strain engineering, etc. The Sn concentration in GeSn has reached the direct–indirect transition point by several groups,[17–22] and some are even much higher, for example 25%[23] and 27%.[24] However, the low growth temperature is a major limitation to obtain device-grade quality materials. The optical property is commonly poor or even no PL is observed for most high Sn concentration samples grown by MBE.[23,25]

In this work, GeSn thin films on Ge (001) with various Sn concentrations from 3.36 to 7.62% were grown by MBE and the structural properties were investigated. It is found that with the increase of the Sn concentration, the crystalline quality degrades indicated by the lateral correlation length (LCL) and the mosaic spread (MS), which would be associated with the drop of optical properties.

EXPERIMENTS

The GeSn thin films with Sn concentration from 3.36 to 7.72% were grown by a 4 inch wafer DCA MBE system on (001) oriented undoped Ge substrates with resistivity of 40 **Ωcm**. The Ge source is an electron beam evaporator, and the Sn source an effusion cell. The absolute flux was calibrated by both electron impact emission spectroscopy (EIES) and crystal oscillation. Prior to the growth, the surface oxide desorption of Ge substrates was carried out by heating the substrate to 550 °C for 30 min in an ultrahigh vacuum chamber. The base pressure in the growth chamber was less than 10^{-10} Torr. The pressure in the growth chamber during epitaxy was in the range of $5-6×10^{-9}$ Torr. After the oxide desorption, a 100 nm thick Ge buffer layer was grown at 500 °C to provide an atomically clean and flat surface. The substrate temperature was then lowered to 200 °C for growth of the 200 nm thick GeSn layer. This growth temperature is below the eutectic temperature of Ge-Sn binary alloys (231.1 °C), which can efficiently restrain the Sn surface segregation. The Ge flux was 0.75 Å/s, and the Sn flux was changed from 0.025 Å/s to 0.6 Å/s for different samples.

The growth process was monitored in real time by reflection high-energy electron diffraction (RHEED) i*n situ* and the surface morphology was investigated by atomic force microscopy (AFM). The structural properties and Sn concentration were analyzed by two-dimensional reciprocal space mapping (2DRSM) in the symmetric (004) and asymmetric (224) planes by high resolution X-ray diffraction (XRD). Furthermore, the LCL and the MS were investigated for the epi-layer peaks in the asymmetric (224) diffraction. MS represents the range of microscopic tilt in the sample. This tilt range causes a broadening of the diffraction feature perpendicular to the line joining the reciprocal lattice point to the origin.[26] LCL represents the full width at half maximum (FWHM) of the layer peak parallel to the interface, which gives an indication of the lateral uniformity of the layer.[27] Moreover, structural properties were also analyzed by transmission electron microscopy (TEM) and Raman scattering measurements. The room temperature Raman spectrum were acquired with a Thermo Scientific DXR Raman microscope, which is in an unpolarized quasi-backscattering geometry by using a diode-pumped solid state (DPSS) laser working at 532 nm, a 1200 lines/mm grating (with ~ 0.8 cm^{-1} resolution), and an air-cooled CCD detector. The penetration depth of the excitation laser in the GeSn thin films is expected to be below 20 nm.[28]

RESULTS AND DISCUSSIONS

FIG. 1. (a)–(f) shows that the surface roughness becomes large with increasing Sn concentration. When the Sn concentration is 3.36% and 3.63%, the sample surface is relatively flat and no Sn segregation is observed. Then, for the sample with 5.63% Sn, pyramid shaped features that are about 20 nm high appear, whose density is about 6×10^8 cm^{-2}. The Sn segregation can be clearly observed when the Sn concentration is above 7%. In FIG. 1. (d) and (e), Sn droplets are observed and become big with increasing Sn concentration. However, when the Sn concentration reaches 7.62%, the Sn droplets become much less, while the pyramids appear again with a higher density ($\sim 3 \times 10^9$ cm^{-2}) and height (~ 50 nm) than that of the sample with 5.63% Sn. FIG. 1. (g) shows the root-mean-square (RMS) roughness of the GeSn sample surfaces. It can be found that the surface roughness gradually becomes large with increasing Sn concentration, and then increases dramatically above 7% (the blue trend line in FIG. 1. (g) intuitively illustrates this change). It is thus estimated that the Sn segregation appears when the Sn concentration is about 5-6%, and 7.62% is the limitation under the current growth conditions, including growth temperature, flux, *etc.*

The structural properties and Sn concentration were analyzed by 2DRSM in the symmetric (004) and the asymmetric (224) diffractions by high resolution XRD. The results of 2DRSM in the asymmetric (224) diffraction are shown in FIG. 2. The vertical dashed-dotted line through the Ge (224) reciprocal lattice point in 2DRSM indicates the trajectory of the (224) reciprocal lattice point of an pseudomorphic growth on a Ge substrate. The diagonal dashed line through the Ge (224) point indicates the trajectory of the (224) reciprocal lattice point of a cubic structure, meaning a strain-relaxed epitaxial layer. It can be observed that separation between the substrate peak and the epi-layer peak becomes large with increasing Sn concentration, due to the increased lattice constant. When the Sn concentration reaches $\sim 7\%$, the epi-layer peak starts to deviate from the vertical direction, indicating onset of strain relaxation. Furthermore, both the substrate peak and the epi-layer peak show an increasing broadening with increasing Sn, indicating degradation in uniformity and irregularity of the GeSn alloy.

From the GeSn layer peaks in 2DRSM, the concentration of Sn atoms and the degree of strain relaxation of the GeSn epi-layer are estimated. The 200 nm thick GeSn epi-layer is fully strained when the Sn concentration is below 7%, while partially relaxed above 7%. FIG. 3. (a) is a TEM image of the sample with 7.6% Sn. Clear threading dislocations marked by the blue circle in the GeSn epi-layer and misfit dislocations by the red circles at the interface of the Ge buffer and GeSn layer can be observed. The generation of dislocations is a proof of strain relaxation in consistent with the phenomena seen in the 2DRSMs.

Furthermore, in order to analyze crystal quality of the GeSn thin film and explain the peak broadening, the LCL and the MS of the GeSn epi-layers were investigated through the analysis of the epi-layer peaks in the asymmetric (224) diffraction. It can be seen from Fig. 3. (b) and (c) that with the increase of Sn concentration, the LCL reduces while the MS increases. MS may arise either because of a fine mosaic structure giving a variation in the tilt of the reflecting plane for different mosaic grains or it may be a result of "rippled" reflecting planes due to the presence of a uniform dislocation
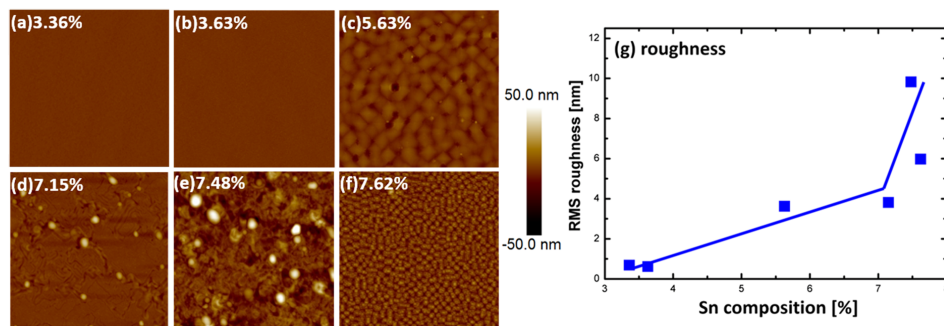

FIG. 1. (a)-(f) AFM 5×5 μm^2 images of the GeSn thin films with different Sn concentrations. (g) Root mean square (RMS) surface roughness of the samples extracted from the AFM images (a)-(f).
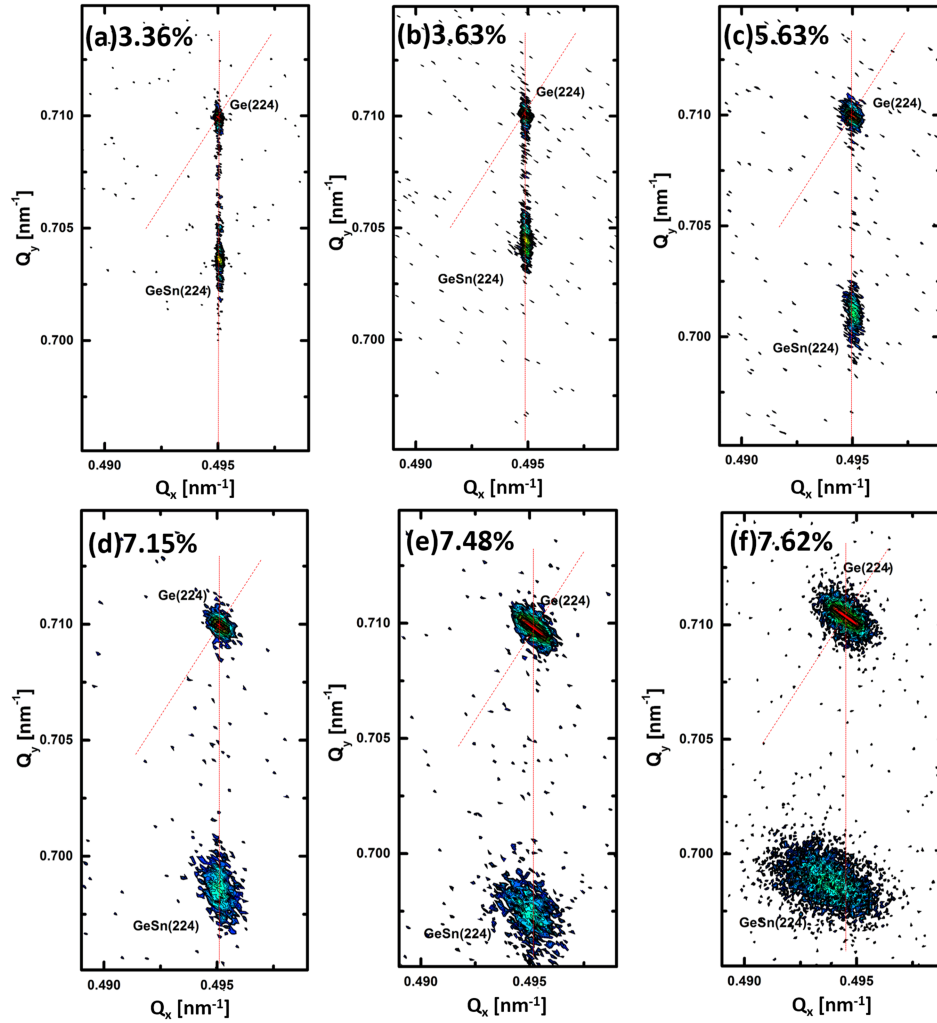
FIG. 2. XRD 2DRSM around (224) diffraction point of the samples with different Sn concentrations from 3.36 to 7.62%. Q_x and Q_y axes are along the [110] and the [001] direction, respectively. The range of Q_x is 0.01 nm^{-1}, and of Q_y is 0.018 nm^{-1} (all ranges are the same for both Q_x and Q_y). The dashed and dashed-dotted lines indicate the situations of fully relaxed and pseudomorphic growth, respectively. The substrate peaks and the GeSn epi-layer peaks are labeled in the figures.

density.[26] From FIG. 3. (a), threading dislocations and misfit dislocations are observed while different pyramid-like features are clearly observed in FIG. 1. (c) and (f) with an obviously different density. These factors are likely the important causes for the MS increasing and peak broadening. LCL gives an indication of the lateral uniformity of the layer. If a layer is perfectly smooth and of uniform thickness in all directions parallel to the interface, the breadth of this peak would be related to an
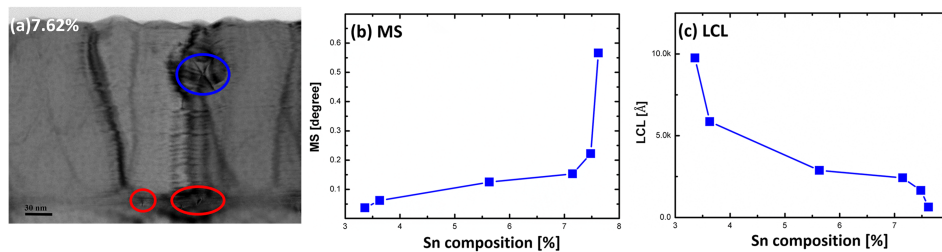

FIG. 3. (a) TEM image of the sample with 7.62% Sn. (b) MS and (c) LCL of GeSn epi-layer peaks from asymmetric (224) diffraction with different Sn concentrations.
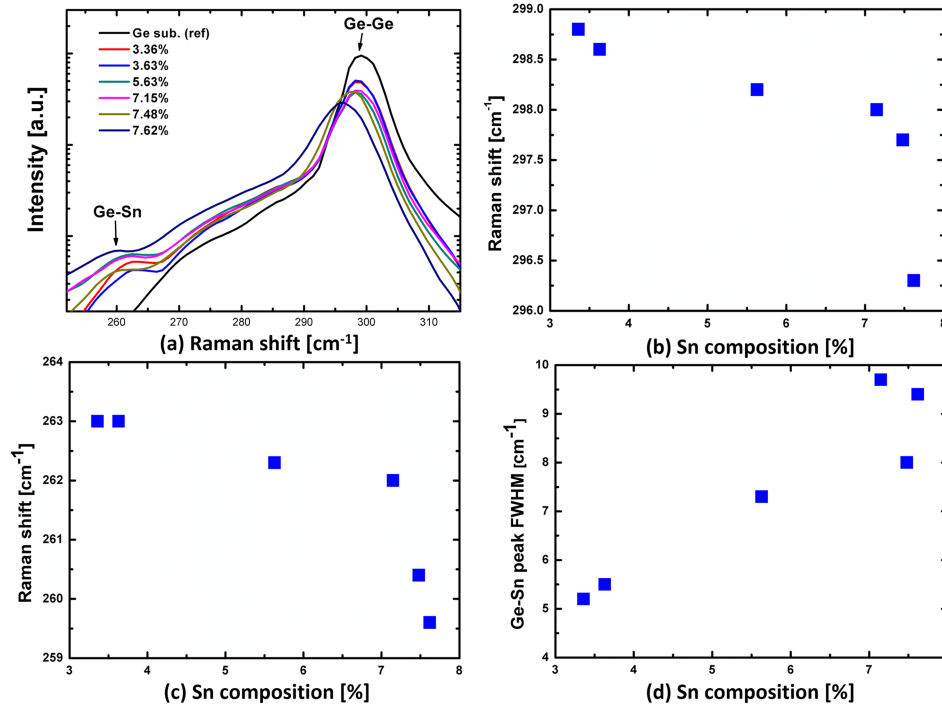
FIG. 4. (a) Raman spectra of GeSn samples. (b) Ge-Ge peak shift, (c) Ge-Sn peak shift and (d) FWHM of the Ge-Sn peaks with different Sn concentrations.

average value of the separation of GeSn thin film lateral irregularities.[27] From FIG. 3. (c), the LCL reduces with the increase of Sn, indicating the lateral uniformity of the epi-layer also decreases. The epi-layer peak broadening is largely due to the increase in Sn concentration, which leads to the decrease of the crystal lattice quality, including strain relaxation with a high dislocation density. Conversely, the decrease of the epi-layer peak crystal lattice quality influences the Ge buffer crystal lattice quality, which causes the substrate peak broadening. Both the LCL and MS show that under the same growth conditions, including growth temperature and Ge flux, GeSn alloy with a higher Sn concentration has a worse crystal quality.

Raman scattering measurements were carried out on GeSn alloys, together with a Ge (001) substrate as a reference. The peaks of the Ge-Ge LO mode and Ge-Sn mode are observed,[18,23,29] and their positions and widths are extracted through multi-peak curve fittings based on a combination of Gaussian and Lorentzian function. Clear shifts can be observed for both peaks at different Sn concentrations. The Ge-Ge peak shifts between 299.8 cm^{-1} and 296.3 cm^{-1}, while the Ge-Sn peak between 263.0 cm^{-1} and 259.3 cm^{-1}. FIG. 4. (b) and (c) show the Raman shift of the two peaks. It is consistent with the published finding that the Raman shift of the Ge-Ge and the Ge-Sn peak vs. Sn concentration roughly follows a linear relationship up to 7%.[18,30] When sample is partially relaxed, the Raman shift is determined by both Sn concentration and the amount of residual strain in the epi-layer, which result in a fast drop in FIG. 4. (b) and (c). The FWHM of the Ge-Sn peak is shown in FIG. 4. (d). With increasing Sn, the FWHM also gradually increases, indicating degradation of the crystal quality, consistent with the results from 2DRSM.

CONCLUSIONS

In this study, GeSn thin films on Ge (001) with various Sn concentrations from 3.36 to 7.62% were grown by MBE. It is estimated that 7.62% Sn concentration could be the limitation at the growth temperature of 200 °C. The structural properties and Sn concentration were analyzed by 2DRSM in the symmetric (004) and asymmetric (224) diffractions by high resolution XRD. With the increase of Sn concentration, the LCL reduces while the MS increases. Both the LCL and the MS show that

under the same growth conditions, including growth temperature and Ge flux, GeSn alloy with a high Sn concentration has larger irregularity. When the Sn concentration is above 7.48%, strain relaxation occurs. Finally, the Raman scattering measurements show broadening of the Ge-Sn peaks at high Sn concentrations. All data indicate the consistent trend that the crystalline quality degrades with increasing Sn concentration, leading to potential degradation of optical properties.

ACKNOWLEDGMENTS

[1] C. A. Mack, IEEE Trans. Semicond. Manuf. **24**, 202 (2011).
[2] M. M. Waldrop, Nat. News **530**, 144 (2016).
[3] R. Soref, Silicon **2**, 1 (2010).
[4] A. Rickman, Nat. Photonics **8**, 579 (2014).
[5] M. V. Fischetti and S. E. Laux, J. Appl. Phys. **80**, 2234 (1996).
[6] S. Gupta, B. Magyari-Köpe, Y. Nishi, and K. C. Saraswat, J. Appl. Phys. **113**, 073707 (2013).
[7] Z. Liu, J. Wen, X. Zhang, C. Li, C. Xue, Y. Zuo, B. Cheng, and Q. Wang, J. Phys. D. Appl. Phys. **48**, 445103 (2015).
[8] X. Gong, G. Han, F. Bai, S. Su, P. Guo, Y. Yang, R. Cheng, D. Zhang, G. Zhang, C. Xue, B. Cheng, J. Pan, Z. Zhang, E. S. Tok, D. Antoniadis, and Y.-C. Yeo, IEEE Electron Device Lett. **34**, 339 (2013).
[9] D. Lei, W. Wang, Z. Zhang, J. Pan, X. Guo, G. Liang, E. S. Tok, and Y.-C. Yeo, J. Appl. Phys. **119**, 024502 (2016).
[10] J. Werner, M. Oehme, M. Schmid, M. Kaschel, A. Schirmer, E. Kasper, and J. Schulze, Appl. Phys. Lett. **98**, 061108 (2011).
[11] M. Oehme, J. Werner, M. Gollhofer, M. Schmid, M. Kaschel, E. Kasper, and J. Schulze, IEEE Photonics Technol. Lett. **23**, 1751 (2011).
[12] S. Wirths, R. Geiger, N. von den Driesch, G. Mussler, T. Stoica, S. Mantl, Z. Ikonic, M. Luysberg, S. Chiussi, J. M. Hartmann, H. Sigg, J. Faist, D. Buca, and D. Grützmacher, Nat. Photonics **9**, 88 (2015).
[13] R. Chen, H. Lin, Y. Huo, C. Hitzman, T. I. Kamins, and J. S. Harris, Appl. Phys. Lett. **99**, 181125 (2011).
[14] E. Kasper, J. Werner, M. Oehme, S. Escoubas, N. Burle, and J. Schulze, Thin Solid Films **520**, 3195 (2012).
[15] S. Zaima, O. Nakatsuka, N. Taoka, M. Kurosawa, W. Takeuchi, and M. Sakashita, Sci. Technol. Adv. Mater. **16**, 043502 (2015).
[16] R. Soref, J. Kouvetakis, J. Tolle, J. Menendez, and V. D'Costa, J. Mater. Res. **22**, 3281 (2007).
[17] H. Lin, R. Chen, Y. Huo, T. I. Kamins, and J. S. Harris, Thin Solid Films **520**, 3927 (2012).
[18] M. Oehme, D. Buca, K. Kostecki, S. Wirths, B. Holländer, E. Kasper, and J. Schulze, J. Cryst. Growth **384**, 71 (2013).
[19] V. R. D'Costa, W. Wang, Q. Zhou, E. S. Tok, and Y.-C. Yeo, Appl. Phys. Lett. **104**, 022111 (2014).
[20] W. Wang, Q. Zhou, Y. Dong, E. S. Tok, and Y.-C. Yeo, Appl. Phys. Lett. **106**, 232106 (2015).
[21] I. S. Yu, T. H. Wu, K. Y. Wu, H. H. Cheng, V. I. Mashanov, A. I. Nikiforov, and O. P. Pchelyakov, AIP Adv. **1**, 042118 (2011).
[22] W. Wang, L. Li, E. S. Tok, and Y.-C. Yeo, J. Appl. Phys. **117**, 225304 (2015).
[23] M. Oehme, K. Kostecki, M. Schmid, F. Oliveira, E. Kasper, and J. Schulze, Thin Solid Films **557**, 169 (2014).
[24] M. Nakamura, Y. Shimura, S. Takeuchi, O. Nakatsuka, and S. Zaima, Thin Solid Films **520**, 3201 (2012).
[25] R. Hickey, N. Fernando, S. Zollner, J. Hart, R. Hazbun, and J. Kolodzey, J. Vac. Sci. Technol. B **35**, 021205 (2017).
[26] P. Fini, H. Marchand, J. P. Ibbetson, S. P. DenBaars, U. K. Mishra, and J. S. Speck, J. Cryst. Growth **209**, 581 (2000).
[27] R. Schad, P. Beliën, G. Verbanck, V. V. Moshchalkov, Y. Bruynseraede, H. E. Fischer, S. Lefebvre, and M. Bessiere, Phys. Rev. B **59**, 1242 (1999).
[28] E. Kasper, M. Kittler, M. Oehme, and T. Arguirov, Photonics Res. **1**, 69 (2013).
[29] V. R. D'Costa, J. Tolle, R. Roucka, C. D. Poweleit, J. Kouvetakis, and J. Menéndez, Solid State Commun. **144**, 240 (2007).
[30] H. Lin, R. Chen, Y. Huo, T. I. Kamins, and J. S. Harris, Appl. Phys. Lett. **98**, 261917 (2011).